

HydroGFD3.0: a 25 km global near real-time updated precipitation and temperature data set

Peter Berg¹, Fredrik Almén¹, and Denica Bozhinova¹

¹Swedish Meteorological and Hydrological Institute, Folkborgsvägen 17, 601 76 Norrköping, Sweden

Correspondence: Peter Berg (peter.berg@smhi.se)

1 **Abstract.** HydroGFD3 (Hydrological Global Forcing Data) is a data set of bias adjusted reanalysis data for daily precipitation,
2 and minimum, mean, and maximum temperature. It is mainly intended for large scale hydrological modeling, but is also
3 suitable for other impact modeling. The data set has an almost global land area coverage, excluding the Antarctic continent and
4 small islands, at a horizontal resolution of 0.25°, i.e. about 25 km. It is available for the complete ERA5 reanalysis time period;
5 currently 1979 until five days ago. This period will be extended back to 1950 once the back catalogue of ERA5 is available. The
6 historical period is adjusted using global gridded observational data sets, and to acquire real-time data a collection of several
7 reference data sets is used. Consistency in time is attempted by relying on a background climatology and only making use of
8 anomalies from the different data sets. Precipitation is adjusted for mean bias as well as the number of wet days in a month. The
9 latter is relying on a calibrated statistical method with input only of the monthly precipitation anomaly, such that no additional
10 input data about the number of wet days is necessary. The daily mean temperature is adjusted toward the monthly mean of the
11 observations, and applied to 1 h time steps of the ERA5 reanalysis. Daily mean, minimum and maximum temperature are then
12 calculated. The performance of the HydroGFD3 data set is on par with other similar products, although there are significant
13 differences in different parts of the globe, especially where observations are uncertain. Further, HydroGFD3 tends to have
14 higher precipitation extremes, partly due to its higher spatial resolution. In this paper, we present the methodology, evaluation
15 results, and how to access to the data set at doi:10.5281/zenodo.3871707.

16 1 Introduction

17 Precipitation (P) and temperature (T) are key driving parameters for many impact models, and there are now many observa-
18 tional data sets available. They differ regarding the spatio-temporal resolution, the historical coverage, and the data sources
19 included in the product. However, when it comes to continuously updated near real-time data sets, there are very few available
20 data sets. It is therefore challenging to find a product suitable for monitoring and initialization of forecasts for an impact model,
21 i.e. a product that fulfills both a long historical period for calibration and validation, as well as real-time updates.

22 While most data sets now offer a rather long historical period, the real-time availability is a greater challenge. Merged satellite
23 and gauge data sets such as CHIRPS (Funk et al., 2015a), CMORPH (Joyce et al., 2004), and PERSIANN-CDR (Ashouri
24 et al., 2015) offer both high resolution and near-realtime components, but are limited to between the +/-50 or +/-60 degree
25 latitude bands. Several data sets have made use of reanalysis data as a basis, adjusted using various gridded observational data

26 sets (Weedon et al., 2011, 2014; Beck et al., 2017; Berg et al., 2018; Cucchi et al., 2020). The advantage is that the reanalysis
27 products are readily available with a large range of variables and output frequencies. Still, the downside with reanalysis products
28 is that especially P is a model product and thereby suffers from model bias. Since the bias can be substantial, several methods
29 have been developed to adjust reanalysis, using different methods and reference data sets.

30 A hydrological operational monitoring or forecast product has strong demands on availability and redundancy of the data
31 flows. The data set HydroGFD1 (Berg et al., 2018) was constructed and made operational for initializations of the hydrological
32 model HYPE (Lindström et al., 2010) for different set-ups across the globe. It offered near-realtime updating of daily P and
33 daily T (mean, minimum, and maximum), until the end of the last calendar month. The real-time components of HydroGFD1
34 were based on ERA-Interim reanalysis, extended by the ECMWF deterministic forecasts, adjusted using monthly mean P
35 from GPCC-Monitoring and GPCC-FirstGuess (Schneider et al., 2018b) products, and monthly mean T from GHCN-CAMS
36 (Fan and Van den Dool, 2008). The follow-up data set HydroGFD2 offered some updates to the methodology, and shifted
37 to using primarily the CPC-Unified (Chen et al., 2008) and CPC-Temp (CPCtemp, 2017) products for P and T adjustments,
38 respectively. Both data sets employed a 0.5° resolution, and have been operationally produced for a few years now, and we have
39 identified some serious issues regarding the availability of required data sets for successful updates. The largest operational
40 intermission occurred during the government lock-down in the US between the 22nd of December 2018 and the 25th of
41 January 2019. Neither of the US data sets included in the production were then available, which hampered the production of
42 the HydroGFD data sets, and subsequently deteriorated the quality of some operational HYPE models. Both these HydroGFD
43 versions have now become obsolete for real-time production due to the discontinuation of the ERA-Interim production as of
44 August 2019. Data sets using multiple input data sources are less sensitive to such conditions, such as the MSWEP data set
45 (Beck et al., 2017).

46 In this paper, the HydroGFD3.0 system is described, with its range of produced data sets for the period 1979 to near real-
47 time, at 0.25° resolution and global land coverage. We describe the methodology and the operational production, as well as an
48 evaluation of the climatological data set, with comparison to other similar data sources.

49 **2 Data**

50 Table 1 lists the data sources used in the production of the different *tiers* (i.e. production lines with different data sets, see
51 Methods section) of HydroGFD3. From now on, we will use the shortened internal abbreviations listed under "Name" in Tab. 1
52 when we refer to the data of P or T from each source. ERA5 is the latest global reanalysis product of the ECMWF (Hersbach
53 et al., 2020) and forms the basis for HydroGFD3. This reanalysis product is chosen because our operational forecasts at SMHI
54 (Swedish Meteorological and Hydrological Institute) are based on the medium range forecasts of ECMWF, with the same
55 model as that used for ERA5, with similar bias, although there are differences in model version. Other reanalysis products
56 would be possible, but are not explored here. ERA5 is updated with a three months lag, but a new temporary product, ERA5T,
57 is produced with a five days lag.

Table 1. Table of model and data sources used in the production of HydroGFD3, as well as the WFDE5 data set used for comparison. Note the lower case abbreviations used in the main text and in figures which follow the internal notation used in the data set production. N_{wet} is a measure of the number of wet days in a month. The data set type is marked in parenthesis in the leftmost column: r - model reanalysis, g - gauge based, s - satellite based

Data set	Name	Variables	Resolution	Period	Reference
ERA5(r)	e5	T, P	1 h; 0.33°	1979–(t-3 months)	Hersbach et al. (2020)
ERA5T(r)	e5t	T, P	1 h; 0.33°	(t-3 months) – (t-5 days)	Hersbach et al. (2020)
CRUts4.03(g)	cru	T, P, N_{wet}	1 mon; 0.5°	1901–(t-2 months)	Harris and Jones (2019)
GPCCv8(g)	gpcc	P	1 mon; 0.25°	1891–2016	Schneider et al. (2018a)
GPCC-monitoringv6(g)	gpccm	P	1 mon; 1.0°	1982–(t-3 months)	Schneider et al. (2018b)
GPCC-First guess(g)	gpccf	P	1 mon; 1.0°	2004–(t-1 month)	Schneider et al. (2018b)
CPC-Unified(g)	cpcp	P	1 d; 0.5°	1979–(t-2 days)	Chen et al. (2008)
CPC-Temp(g)	cpct	T_{min}, T_{max}	1 d; 0.5°	1979–(t-2 days)	CPCtemp (2017)
CHPclimv1.0(g,s)	chpclim	P	clim.; 0.05°	(1980–2009)	Funk et al. (2015b)
WFDE5-CRU(r, g)	wfde5-cru	T, P	1 h; 0.5°	1979-2018	Cucchi et al. (2020)
WFDE5-GPCC(r, g)	wfde5-gpcc	P	1 h; 0.5°	1979-2016	Cucchi et al. (2020)

58 As described in Section 3, HydroGFD3 is based on a combination of the ERA5 reanalysis with the different data sets as
59 listed in the top section of Tab. 1. In the following analysis, we compare the different data sets included in the processing, and
60 additionally make a state-of-the-art comparison to the data set WFDE5 (Cucchi et al., 2020), which is a new product using the
61 *WATCH forcing data* methodology (Weedon et al., 2011) with ERA5 reanalysis, listed in the bottom section of Tab. 1.

62 An issue with global scale evaluations is that of independence between data sets, and most of the gauge-based data sets
63 listed in Tab. 1 make use of more or less the same openly available observations, with regional differences. The data sets have,
64 however, been independently generated and use different statistical models for the gridding process. Our aim is to provide a
65 comprehensive overview of HydroGFD3 in comparison to other data sets, in order to presents its qualities and to point out
66 potential issues. For each of the comparisons in Section 5, we chose data sets that are as independent as possible, given the
67 limitations just discussed. Our experience from earlier studies is that in-depth evaluation can only be performed at the local
68 scale (e.g. Fallah et al. (2020)), and we encourage users of the data set to pursue such evaluations.

69 3 Method

70 The main method that HydroGFD is building on consists of adding observational monthly anomalies to a background climatol-
71 ogy, then adjusting the reanalysis data to that absolute monthly mean. Time steps shorter than the monthly mean are implicitly
72 adjusted following the monthly scaling. A monthly time scales is adopted due to the generally higher availability of obser-
73 vational data sets at this resolution. Further steps assure consistency between different versions of the data set, e.g. regarding
74 spatial coverage. The different steps in producing the HydroGFD3 data sets are presented in detail in the following sections.

75 3.1 Climatology

76 The P background climatology is based on chpclim climatology of satellite, gauge, and physiographic indicators (Funk et al.,
77 2015b). We retain the same climatological period (1980–2009) throughout the HydroGFD3 data set. chpclim comes in two
78 versions, one with full coverage for the 50°S–50°N latitude band, and one with global land coverage. We choose to make
79 the global coverage version the main choice, but add information from the tropical full coverage version to increase coverage
80 along coastlines and islands. The original 0.05° resolution is remapped to the 0.25° resolution of the HydroGFD3 dataset,
81 ensuring conservation of precipitation totals. Some issues with the chpclim data set were identified through visual inspection,
82 with observational artifacts in mid-northern Siberia, and underestimation in Scandinavia. Therefore, these two regions were
83 replaced by gpch climatology data for the 1980–2009 period (see supplementary material for details). To avoid introducing
84 sharp borders, a zone of five grid points were used around each area as a linear transition from one data set to another. Since
85 Greenland P is poorly mapped by both satellite and gauge data, we have chosen to let its climatology be defined by e5, rather
86 than any of the data sets.

87 For T , we use the cpct climatology (1980–2009) with only a remapping to the 0.25 degree resolution, and in-filling of
88 missing data points using e5. The third climatology consists of the wet day frequency (1980–2009), which is taken from the
89 N_{wet} of the cru data set of gridded station observations of the number of wet days in a month. Both T and P are remapped to
90 the 0.25° resolution, using a bilinear interpolation method.

91 In a final step, the three climatologies are harmonized by only retaining the grid points that are available consistently in
92 all data sets and all months. This leads also to the final land-mask of the HydroGFD3 data set, for which adjusted data are
93 produced.

94 The elevation is defined by the e5 surface geopotential divided by the gravity of Earth (9.80665 m/s²).

95 3.2 Anomaly method

96 HydroGFD3 makes use of several different data sets, which need to be stitched together in different configurations depending
97 on the use. Without some kind of homogenization between the data sets, sharp changes in the data are unavoidable when
98 switching from one data set to another. The homogenization used here is performed by only making use of anomalies from the
99 different data sets.

100 In the earlier version HydroGFD1 (Berg et al., 2018), which is closely based on the WFD method (Weedon et al., 2011), each
101 month of the reanalysis data set is adjusted with the absolute monthly mean of the observational data set. This main principle is
102 retained, however, in a new homogenization step we create new absolute observations by first calculating the monthly anomaly
103 compared to the 1980–2009 climatological period calculated for each data set, then adding this anomaly to the HydroGFD3
104 climatology. Anomalies are additive for T

$$105 T_{anom}(year, month) = T(year, month) - T_{clim}(month) \quad (1)$$

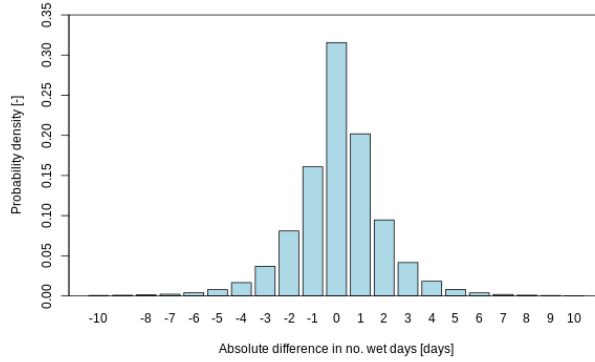


Figure 1. Distribution of the absolute difference in the number of wet days N_{wet} estimated through the Stillman and Zeng (2016) method, and gpcch P . The probability density function ranges globally over all land grid points.

106 and multiplicative for P

$$107 \quad P_{anom}(year, month) = P(year, month) / P_{clim}(month) \quad (2)$$

108 The reverse operation is applied after replacing the climatology.

109 3.3 Wetday frequency

110 A common issue with coarse resolution models, such as e5, is a tendency to produce excessive drizzle that reduces the number
 111 of dry days in a month. To alleviate potential excessive drizzle, the number of wet days are adjusted before correcting the P
 112 amount. This is performed by first determining the target number of wet days in the month, then setting the days with weakest
 113 precipitation intensity to zero until the target is reached. No adjustments are made for too few wet days. The wetday frequencies
 114 in a month are not well covered by observational monitoring records and the uncertainties are large when available. We have
 115 chosen to estimate the number of wet days based on the method of Stillman and Zeng (2016). Note that we do not need to
 116 define a wet day using a specific threshold value. Instead, the number of wet days in a month are directly defined by the method.
 117 The method essentially relates the number of wet days, N_{wet} , to the monthly P anomaly, P_{anom} , using also the climatological
 118 wet day frequency (calculated from cru wet days data set), N_{wet}^{clim} as a predictor, and a tunable constant, k .

$$119 \quad N_{wet} = P_{anom}^k * N_{wet}^{clim} \quad (3)$$

120 A value of $k = 0.28$ was derived for HydroGFD2.0 by calibration to the cru observations of the number of wet days in a
 121 month, together with the cpcp P observations. This value is almost half of that found by Stillman and Zeng (2016), which can
 122 probably be related to the data sets used, but was found to be well applicable across the world. A verification of this constant
 123 was performed with the cru wet days and the gpcch monthly P anomalies, see Fig.1. This reveals an overall high accuracy of
 124 the method, with deviations from observations of mostly only few days in a month, but can in rare cases be as much as ten

125 days. On average over the 1980–2009 period, and for each single grid point, the deviations are close to zero. Thus, the method
126 works well across all areas, and with sufficient precision for our purposes.

127 **3.4 Applied corrections**

128 The production of the corrected data consists of the following steps.

- 129 1. Calculate observed anomalies
- 130 2. Construct absolute reference data by adding the anomalies to the HydroGFD3 climatology
- 131 3. (*P* only) Calculate the number of wet days
- 132 4. (*P* only) Remove the weakest excessive wet days in e5
- 133 5. Calculate the ratio (for *P*) or difference (for *T*) between the monthly means of the reference and e5
- 134 6. Apply the ratio or difference to all time steps of e5 within the month
- 135 7. (*T* only) Calculate mean, minimum, and maximum *T* from the hourly time steps

136 For *P*, the scaling can cause very large values in some cases, e.g. when e5 severely underestimates the number of wet days.
137 Therefore, *P* is limited to a maximum of 1500 mm/day, which is close to the highest observed record at that time scale.

138 **3.5 Consistency in time and space**

139 To have consistent output in all versions of HydroGFD3, there are internal checks to verify that each of the defined grid points
140 of HydroGFD3 is receiving data after each monthly adjustment. It happens that the land sea masks of the observational data sets
141 change over time, and they often differ between different data sources. If the anomaly data is not defined for a particular grid
142 point, a search algorithm will identify if there are defined anomalies in grid points within a 5 grid box radius. If the search is
143 successful in finding at least one value, the mean of all values in the search radius is used to fill the grid point value. However,
144 if no defined data is found, the anomaly will be set to 0 for *T* and 1 for *P*; in other words, the adjustment will be toward the
145 HydroGFD3 climatology.

146 **3.6 Evaluation**

147 Evaluation of the HydroGFD3 historical data set is presented for the mean climatology of *P* and *T*, as well as for regional
148 probability distribution functions (PDF) of daily data and as monthly mean time series. The two latter evaluations are performed
149 for each of the regions defined by Giorgi and Bi (2005) (although we use the correct longitude and latitude coordinates provided
150 by Huebener and Körper (2013)) commonly referred to as Giorgi regions, see Fig. 2. One exception is that we have left out the
151 EQF region in the plots of PDFs, since it is contained in other included regions. The reason is that it overlaps other regions,
152 and having only 25 regions simplifies the presentation layout of the plots substantially. For both the PDFs and the time series,

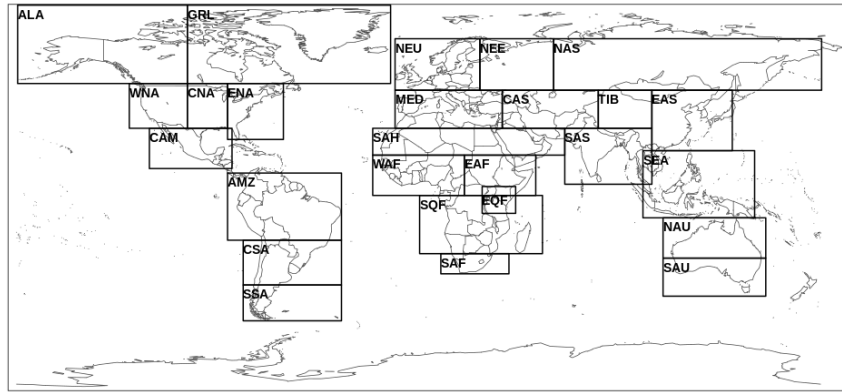


Figure 2. Evaluation regions as defined by Giorgi and Bi (2005), and employed in the PDF and time series analysis.

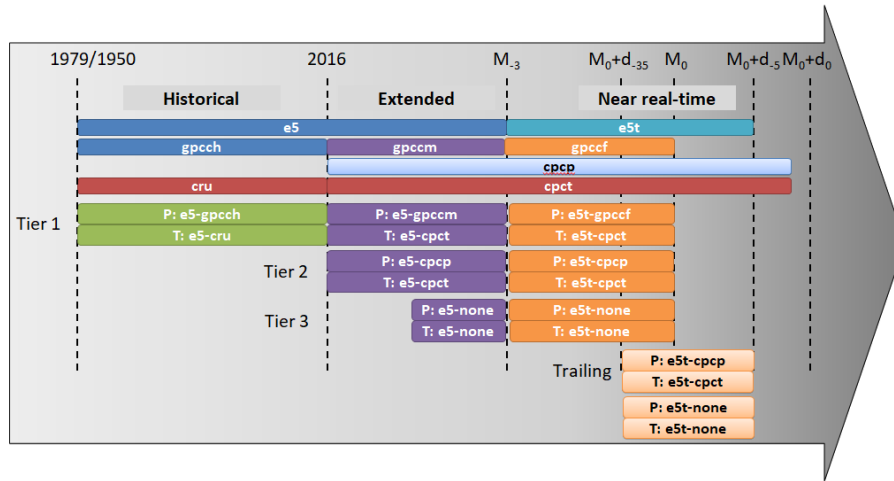


Figure 3. Schematic of the different HydroGFD3 products on a non-linear time axis. The top bars show the original data sources, and the Tier 1–3 and Trailing products are shown below. Abbreviations follow Tab. 1. The time axis denotes years with significant changes in data sources, and the later time marks are relative to the 1st of the current month, M_0 , and the current day, d_0 . The units of the sub-script for the month is in months, and for the day is in days.

153 only data points in the defined grid points of HydroGFD3 are used. The PDFs are pooling all data in each domain, whereas the
 154 time series plots are based on regional averages for each monthly time step.

155 4 Data sets

156 HydroGFD3 is built up by different data sets depending on the time period and the tier, see schematic in Fig. 3.

157 The historical period (1979–2016) is built on e5 corrected with the gpcc and cru data sets, respectively for P and T . There
158 is only one tier produced for this period. e5 will later be released back to 1950, and the HydroGFD3 historical data will then
159 cover that period as well.

160 After 2016, in the "extended" and "near real-time" periods, there are three tiers built on different data sets. Tier 1 is the
161 primary choice and follows the gpccm (for the e5 period) and gpccf (for the e5t period) products for P adjustments, and the
162 cpct product (for the complete period) is used for T . Tier 2 builds instead on the cpcp and cpct products. Note that the Tier 1
163 and Tier 2 T products are identical, and are only repeated here for simplification of the schematic. In practice, there is no Tier
164 2 for T , and the tiers are anyway not necessarily used consistently for T and P together, since the data sets are completely
165 independent. Tier 3 is the final resort if none of the data sets for a variable is available. It is performing only a climatological
166 correction of e5 or e5t by calculating anomalies of the reanalysis and adding/multiplying this to the HydroGFD3 climatology.
167 Since it does not make use of any observational data sets, it has received the internal file naming convention "none". For P , also
168 the number of wet days is adjusted, according to the description in Section 3.3, using the reanalysis anomalies as a predictor.

169 A closer to real-time product is possible, with the daily time step cpcp and cpct products being available with a two day
170 latency, and e5t available at five day latency. The adjustment of the e5t data is then based on the latest available 30 days,
171 synchronized between the data sets, and is therefore called "Trailing".

172 4.1 Operational aspects

173 The HydroGFD3 data sets are updated at regular intervals. The "extended" period is updated each month, as new e5 and other
174 data sets become available. Each tier works independently, and can therefore become available at different times.

175 The "near real-time" period is updated at earliest five days into the new month, when e5t is available. By then, the cpcp
176 and cpct products are generally available, but gpccf normally needs a few days more. Tier 3 needs no additional data sets,
177 and is available together with e5t, but is produced at the calendar month timestep like the other products. The priority order is
178 independent for each variable, and goes from Tier 1–3.

179 Finally, the "Trailing" updates are performed along with e5t and cpcp and cpct updates, and is normally available at a five
180 days time lag.

181 5 Results

182 5.1 Climatology

183 The climatological period of HydroGFD3 is set to 1980–2009, and is consistently used in this section. Figure 4 presents the
184 annual mean climatology of HydroGFD3 for both P and T , as well as the bias of the e5 reanalysis to this climatology. e5 has
185 in general a wet and cold bias in mountainous regions in most of the world. The Arctic is generally wetter and warmer in e5;
186 note that Greenland P is bias free per definition since the HydroGFD3 climatology uses e5 there. The tropics are generally
187 drier and colder in e5.

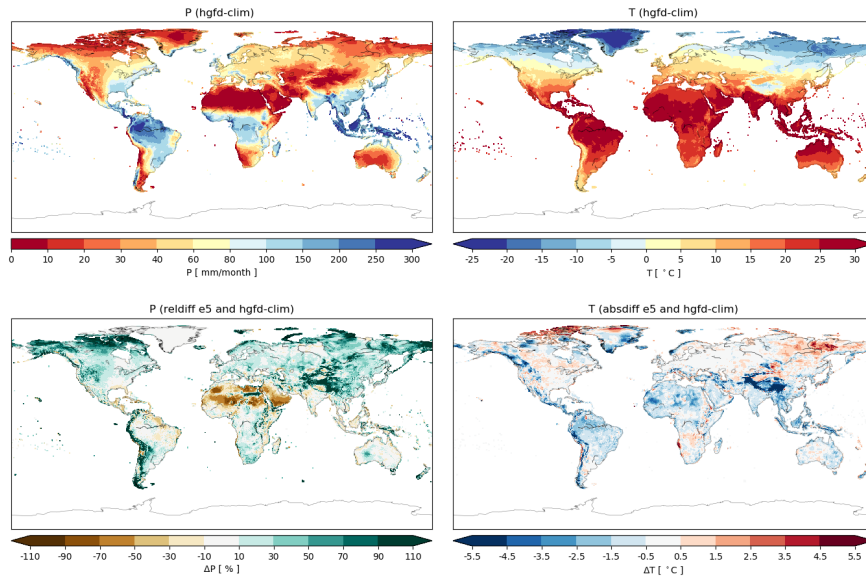


Figure 4. The baseline HydroGFD3 annual mean climatology for P (top left) and T (top right). The bottom row shows the bias of the e5 reanalysis for each variable to the climatology. Note that the lack of P bias for e5 in Greenland is due to the definition of using e5 climatology for that region.

188 Figures S1–S4 show the seasonal HydroGFD3 climatology and biases of e5. The bias patterns are rather stable across the
 189 seasons, although the magnitude changes somewhat. Most striking are the relative changes in western Africa in the December–
 190 February period, but this is the dry period there and the relative changes are therefore comparing low numbers which tend to
 191 exaggerate the absolute term differences.

192 We also compare the HydroGFD3 climatologies to other data sets, mainly with a focus on data with daily time steps that
 193 could be used equally for the historical period, but also to gpcch, which is the main background data set for anomalies in
 194 the historical period. Figure 5 shows the annual mean difference in P of gpcch, cpcp, wfde5-gpcch, and wfde5-cru to the
 195 HydroGFD3 climatology. Differences to gpcch are generally within $\pm 10\%$, except for parts of the Andes mountain range,
 196 the Canadian Arctic, the dry north of Africa, the Himalayan plateau, and Greenland. These are all dry and/or snowy regions,
 197 with an inherent observational uncertainty, adding the lower gauge network density in the areas. The presented differences
 198 between the data sets are considered well inside this expected uncertainty range. We also remark that uncertainties in Greenland
 199 are especially large due to few observations and difficult conditions, and data for this region should be used carefully, with
 200 HydroGFD3 and other data sets alike. The cpcp data set is generally drier, especially in the Arabian peninsula. wfde5-gpcch and
 201 wfde5-cru are both generally wetter than the HydroGFD3 climatology, especially in the cold seasons (see Fig. S5–S8). This is
 202 due to the gauge corrections applied in the wfde5 data, which is also the reason for wfde5-gpcch not being identical to gpcch,
 203 which it is based on. There are also discrepancies in large dry desert areas such as Sahara desert, which arise due to differences
 204 in the way the number of wet days are calculated in the different data sets. The WFDE5 implementation would produce NaN in

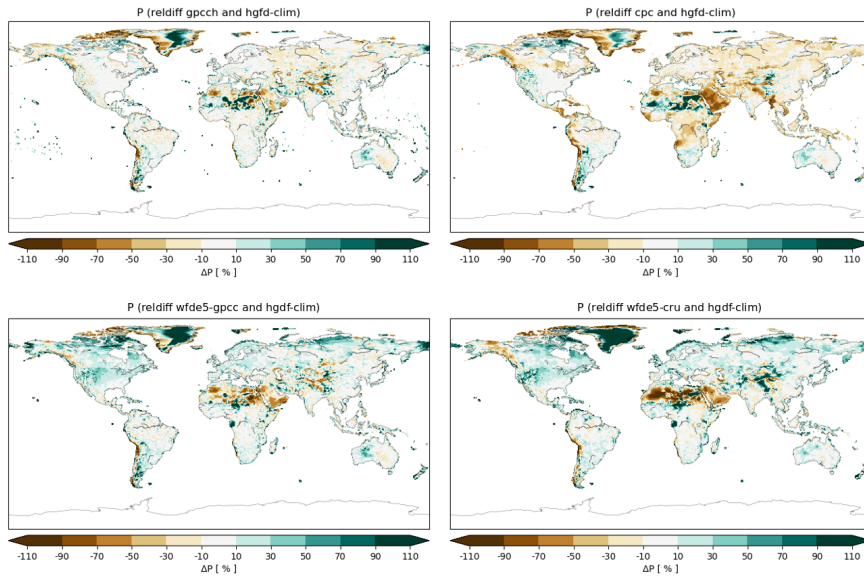


Figure 5. Relative difference of data sets to the HydroGFD3 annual mean P climatology for the period 1980–2009; gpcc (top left), cpcp (top right), wfde5-gpcc (bottom left) and wfde5-cru (bottom right).

205 division by zero if the number of wet days was zero, which has not happened so far (reviewer comment by Graham Weedon).
 206 In HydroGFD3, division by zero does occur, and is solved by setting the ratio to zero when the calculated number of dry days
 207 equals zero. An incompatibility between P and no observed wet days can act to remove P completely for some months, and
 208 therefore making a drier data set. Seasonal differences (Fig. S5–S8) show similar patterns as the annual mean for most of the
 209 regions, but can also differ substantially in some regions. One region that stands out is southern Africa in JJA, where both
 210 gpcc and cpcp show much wetter conditions (Fig. S7).

211 For T , we compare to cru only, since cpct is used to build the climatology on top of which cru anomalies are added, and
 212 wfde5-cru is adjusted to cru and is per definition identical regarding climatology. Fig. 6 shows the absolute difference of cru
 213 and the HydroGFD3 climatology for each season of the climatological year. The largest differences are in the Arctic region
 214 where gauge availability is low. In other regions, such as central-south Africa, the Himalayan plateau, and other orographic
 215 regions, the differences are very consistent over all seasons, with deviations up to a few degrees Celsius. This makes us suspect
 216 that they are due to differences in the elevation used for the different data sets. The cpct data set does not come with any
 217 information on the elevations used. The use of anomalies from the cru and cpct in constructing the final data set removes such
 218 effects, but the climatological difference remains.

219 5.2 Distributions

220 Figure 7 shows the PDFs for the complete time period 1980–2009 for P , and for each of the data sets e5, hgfd3, cpcp, wfde5-
 221 cru and wfde5-gpcc. In these plots, the spread between the coloured lines representing direct observations or e5 adjusted to

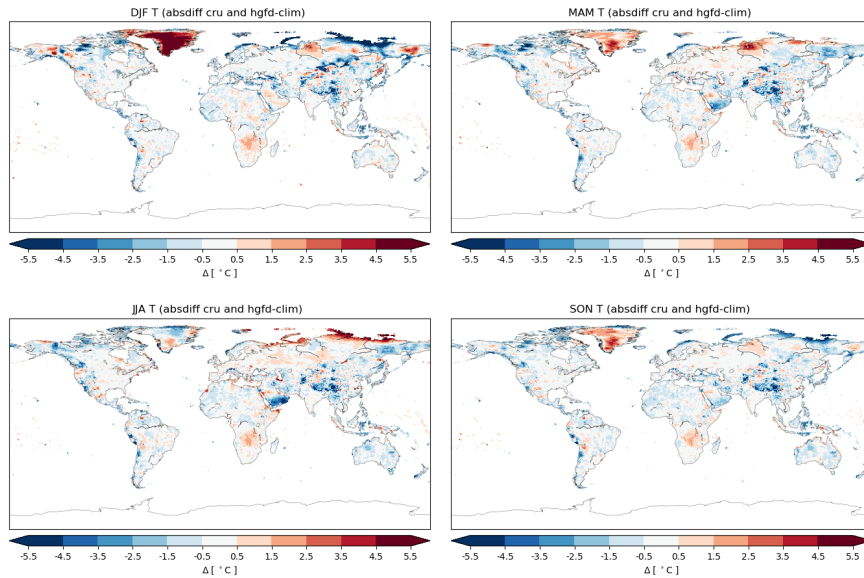


Figure 6. Absolute difference T climatology for the period 1980–2009 between cru and HydroGFD3 for each season (top left) December–February, (top right) March–May, (bottom left) June–August, and (bottom right) September–November.

222 observations, can be interpreted as indicators of the uncertainty in the observed state. Many regions show fairly high agreement
 223 between the datasets, including the e5 original data. In some regions, there is a large spread in the observations, and e5 is
 224 somewhere in between, e.g. in ALA, GRL, TIB, and SAH. Again, these regions have large observational uncertainty, making
 225 it difficult to determine a ground truth. However, in other regions e5 is deviating significantly in part of the distribution, such
 226 as in SSA and WAF moderate intensities, AMZ and EAF extreme intensities.

227 HydroGFD3 tends to have higher extremes than other datasets. This is partly a resolution effect due to the 0.25 degree
 228 resolution of HydroGFD3, and 0.5 degree of the other data sets used here. A coarser resolution will move all higher intensities
 229 toward the lower intensities (to the left in the PDF plots). That the effect differs between regions is because the extremes are
 230 also modulated by the magnitude of the applied correction, i.e. the applied scaling. A scaling factor above one will increase
 231 the extremes, and below one will decrease them. The baseline climatology therefore has an impact on the extremes. Also the
 232 wet-days calculation of HydroGFD3 can affect the results, and we find that the dry regions, e.g. SAH and MED, has more
 233 dry days in HydroGFD3 than in the other data sets. When e5 only gives few P days, while the observational anomaly is
 234 high, the scaling factor can become very large, and the only process to limit this is the upper limit of 1500 mm/day, which
 235 is seldom reached. The wfde5-gpcc, which has a similar methodology as HydroGFD3, still has lower extremes. Besides the
 236 above mentioned under-catch corrections, the lower extremes may be due to the upper threshold applied to each hour, as can
 237 be seen in the original wfde5-code in the CDS-catalogue (<https://doi.org/10.24381/cds.20d54e34>).

238 For T , the general shapes of the PDFs agree across all data sets and regions (Fig. 8). However, there are sometimes substantial
 239 differences between e5 and the observational data sets. Typically, e5 displays issues around 0 °C, which is common in global

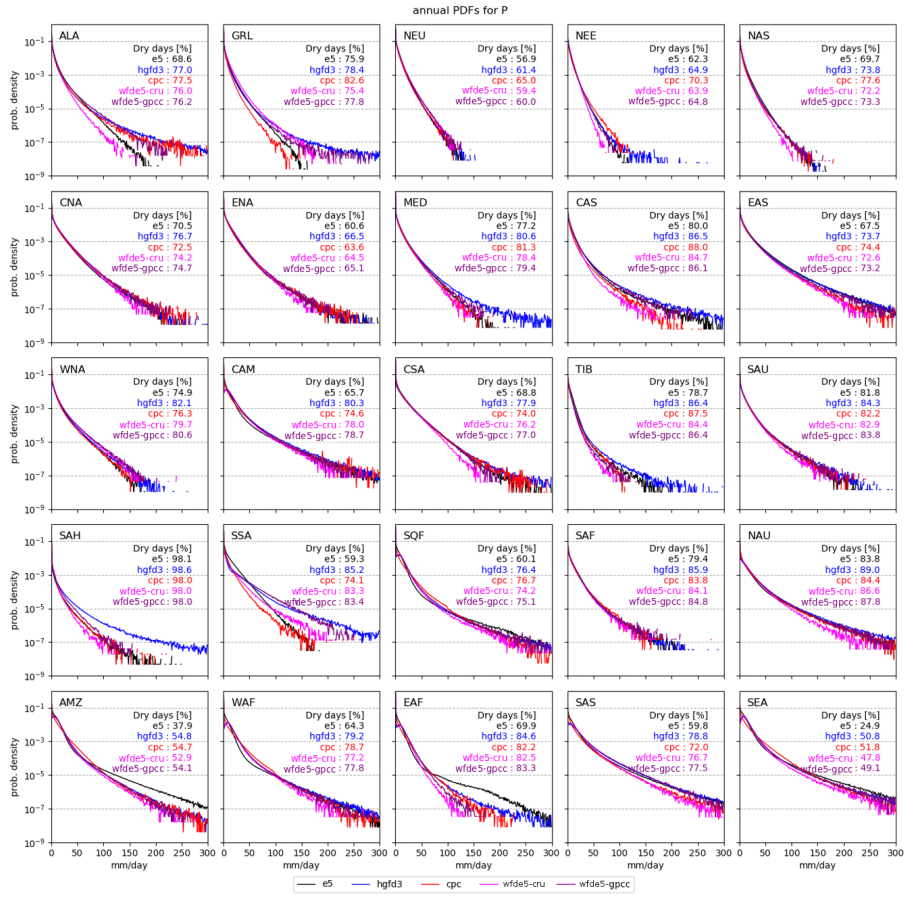


Figure 7. P PDFs of each Giorgi region for the data sets with daily output data in the period 1980–2009. The table in each plot states the percentage of dry days for each data set, i.e. the percentage of data in the first bin of 0–1 mm/day.

240 models and related to melting conditions. There are also seasonal offsets outside the range of the observations. HydroGFD3
 241 remains fairly close to cpct and wfde5-cru in most cases. Orographic effects on T were not accounted for in this comparison,
 242 which can explain some of the differences in regions with varying orography such as TIB.

243 5.3 Temporal trends

244 To get an impression of the temporal trends, and to identify potential issues in the time series, we also investigate the time series
 245 as an average over the Giorgi regions. To emphasize differences between the data sets, we discuss mainly differences relative
 246 to a common reference, here chosen to be e5. In other words, we present the inverse bias of e5 compared to each observational
 247 source.

248 Figure 9 shows the results for P for the period 1980–2019, and the absolute values are shown in Fig. S9. Note that wfde5-
 249 gpcc ends in 2016, wfde5-cru ends in 2018, and gpccm and gpccfg are only available for the last years. The most striking

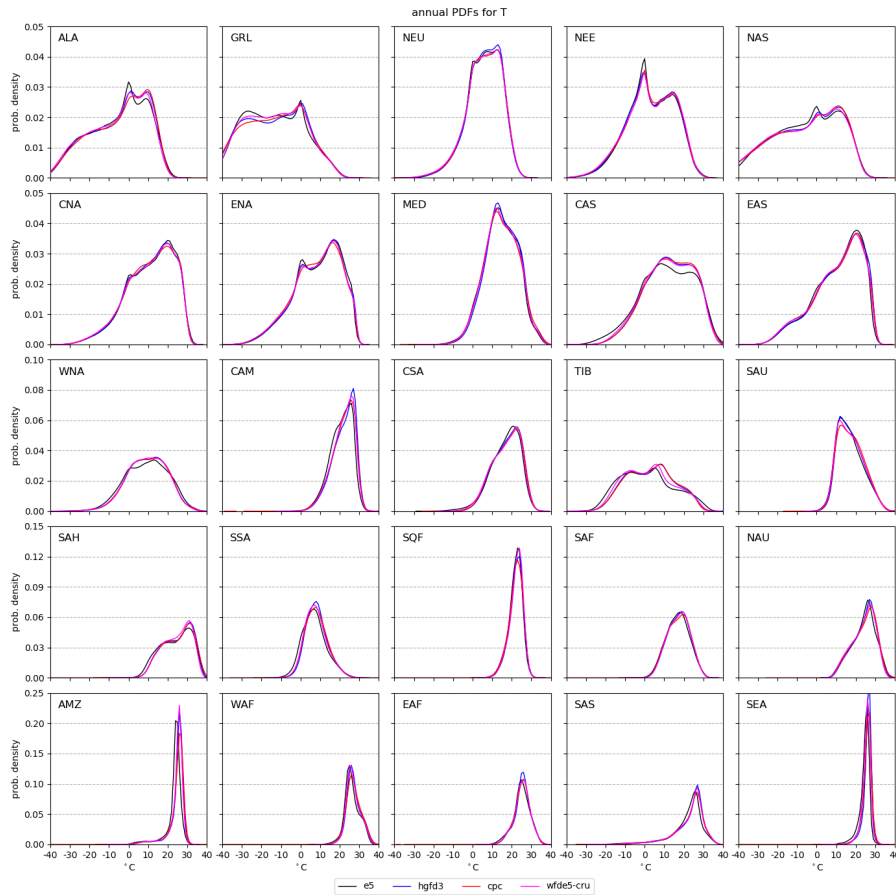


Figure 8. T PDFs of each Giorgi region for the data sets with daily output data in the period 1980–2009.

250 feature is the strong deviations of cpcp for many of the regions. It also varies significantly with time by changing variance,
 251 e.g. in SEA, changing mean value, e.g. in CAS, SAS, and AMZ. In some years, there are significant offsets compared to
 252 surrounding years, e.g. in 2014 in NEU, NEE, CAS and MED. Likely, these issues are due to variations in the underlying
 253 station network, but we have not verified this. All data sets show signs of an annual cycle in their anomalies to e5 in colder
 254 regions, which is indicative of differences between warm and cold season precipitation. wfde5-gpcc and wfde5-cru display
 255 stronger anomalies over the annual cycle in the colder regions compared to other data sets. This is likely due to the undercatch
 256 corrections which are larger for snowy conditions. As expected, HydroGFD3 follows the general trends of wfde5-gpcc, and
 257 the other data sets have similar trends, besides the cpcp deviations just discussed. The gpccm and gpccf have similar mean and
 258 variance as gpcc in the overlapping period, and show generally consistent behavior for the later years. Although, some larger
 259 anomalies occur in, e.g., CAN, CAM, SQF, and SAH.

260 For T , the anomalies to e5, see Fig. 10 (and Fig. S10), retain a clear annual cycle in many regions. Sometimes, the annual
 261 cycle is mainly for wfde5-cru (e.g. NEU, TIB, SAS), but often for all data sets. HydroGFD3 and cpct are in general close to

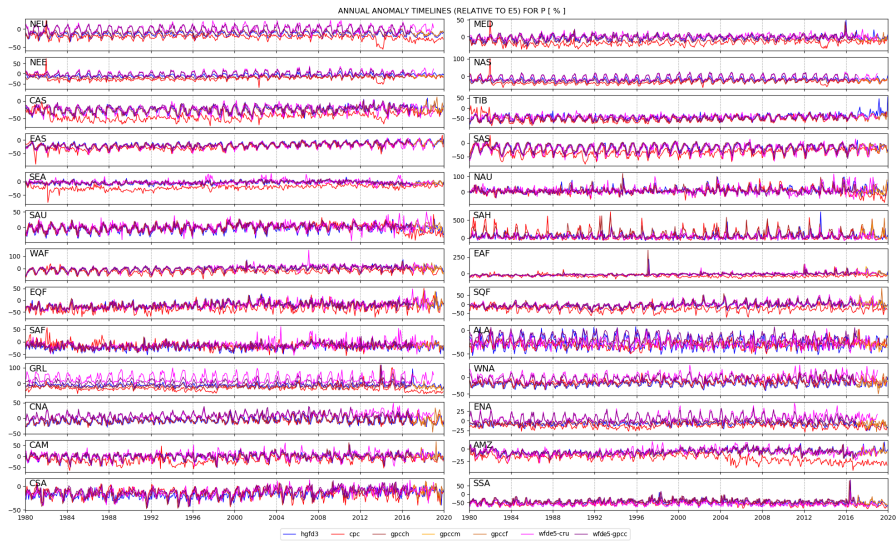


Figure 9. Monthly P anomalies for all data sets, averaged over the Giorgi regions for all valid land data points. The anomalies are relative to the e5 data set, and are evaluated for each single month.

262 each other, because of the HydroGFD3 climatology reducing the offset to zero. However, cpct has some clear "break points" in
 263 its time series in some regions. For example, in NEU, there is a marked change in the magnitude of the anomalies from about
 264 0 to 0.5 °C to -0.5 to 0.5 °C about year 2006. A similar change about that time is visible also for EAS, GRL, MED, SAS, and
 265 NAU. Because the climatologies are calculated for the period 1980–2009, part of these changes are included with the earlier
 266 weaker variability. HydroGFD3 is based on cru anomalies pre-2016, but from 2016 on, also its variability is subjected to the
 267 changes in cpct.

268 Some regions display a significant offset between the data sets, such as SEA, CSA, MED, TIB, and SAS, with cru having
 269 generally lower T_s . Interestingly, changes in cpct after 2006 often act to reduce the offset to e5.

270 5.4 Extending to near real-time

271 The near real-time products, in Fig. 3 called "trailing", use the daily updates of the cpcp and cpct observations. They are
 272 therefore subject to the quality of the cpc products, and the changes in time as discussed in the previous section. This product
 273 follows HydroGFD3 fairly closely to that shown in Fig. 9 and 10, as the main version Tier 2 is also based on cpcp and cpct,
 274 but with corrections at calendar months.

275 In addition, also the "none" products are created with the trailing time window. These only replace the e5 climatology with
 276 that of HydroGFD3, and is the simplest form of corrections of the mean. They act as the last failsafe option in the production
 277 chain, before defaulting to un-corrected e5 data. We do not present this product in the time series plots, since it would only
 278 constitute a constant annual cycle offset in comparison to e5.

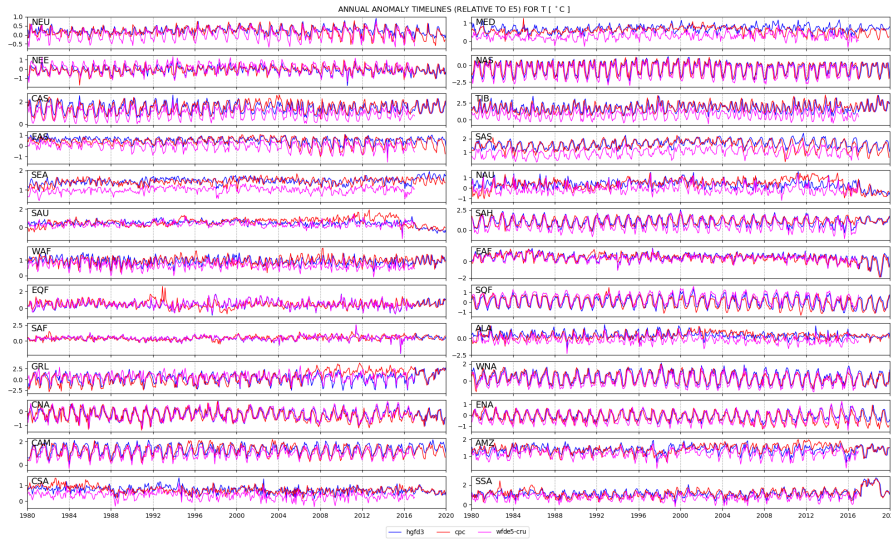


Figure 10. Monthly T anomalies for all data sets, averaged over the Giorgi regions for all valid land data points. The anomalies are relative to the e5 data set, and are evaluated for each single month.

279 6 Discussion

280 Compared to similar data sets based on reanalysis, such as WFDE5 and MSWEP, HydroGFD3 differs in that it has its own
 281 climatological background, and performs the corrections based on anomalies of that same climatological time period. The
 282 reason for using this method, is to be able to switch data sets closer to real-time, without "jumps" in the time series. This works
 283 well as long as the real-time data set retains its climatological state, which seems to be the case for gpcem and gpcem compared
 284 to gpcch. However, cpct and cpcp both cause issues due to changes in the time series towards the end of the time period, about
 285 year 2006. The bias of e5 is still reduced, which brings validity to the method. A future development could be to instead retain
 286 trends from the ERA5 reanalysis, and explore the use of shorter periods for calculating anomalies of the observed data. This
 287 would reduce discontinuities in the time series, but would remove the potential benefits of using trends from the observations.

288 HydroGFD3 has generally higher extremes than the other analyzed data sets. This is especially so in drier regions where an
 289 interplay between the estimation of the number of wet days and the scaling causes fewer wet days and larger scaling factors.
 290 In effect, this leads to enlarging the tail of the distribution, e.g. in the MED and SAH region in Fig. 7. It is possible to restrict
 291 the scaling by only allowing the scaling factor to be a few times the original value, but such restrictions would in turn impact
 292 on the monthly mean. A potential method would be to "borrow" P from adjacent grid points on e5's excessive dry days, and
 293 thereby reducing the scaling factors. This topic is being investigated for future updates of the methodology.

294 The regional analysis shows clearly that the observational data sets give substantially different results in some regions.
 295 Diverse results are more common in data sparse regions or in regions where data are not generally available to all data sets. It is

296 therefore difficult to determine which is closer to the truth in a global assessment like this, and more detailed regional studies,
297 such as Fallah et al. (2020), are needed.

298 The current main usage of the data set is to initialize different HYPE forecasting models around the world, e.g. in Europe
299 (Hundecha et al., 2016), the Niger river (Andersson et al., 2017), and world-wide (Arheimer et al., 2020). This has influenced
300 some of the choices for the setup, such as the use of only the ERA5 reanalysis model, among other reanalysis systems used
301 in e.g. the MSWEP data set (Beck et al., 2017). The forecasts produced by these hydrological models are primarily using the
302 ECMWF deterministic medium range forecasts, or the probabilistic SEAS5 seasonal forecasts, which both use the same model
303 as e5. The priority order of the different redundancy options, i.e. the Tiers 1–3, is based on experience with using the different
304 data sources for our forecasts, with impact from both availability for a given month as well as experienced longer interruptions.

305 **7 Conclusions**

306 The HydroGFD3 methodology of correcting the e5 reanalysis model toward an observational reference, along with the resulting
307 data sets were presented. We conclude that the data sets compare well with existing similar data sets.

308 The main new features of HydroGFD3 are:

- 309 – Higher spatial resolution of 0.25 degrees.
- 310 – Near real-time corrected data until five days from now, i.e. following the continuous updates e5 + e5t time period.
- 311 – Temporal coverage from 1979, and will be extended back to 1950 along with the extended e5 data expected during 2020.
- 312 – Multiple redundancy options to avoid halting production when single data sets are delayed.

313 **8 Data availability**

314 A historical period, ranging from February 1979 to December 2019, is available as open source from the ZENODO repository
315 at doi:10.5281/zenodo.3871707. For years prior to 2017, cru and gpccm are used as reference data for T and P , respectively.
316 The following years use instead cpct and gpccm reference data.

317 Real-time updates of the data set are available for a processing charge via subscriptions. Please make a request here:
318 <https://hypeweb.smhi.se/buy-water-services/data-subscription/> and make sure to mention the data set name "HydroGFD3".

319 *Acknowledgements.* The authors would like to thank the EU and the Swedish Research Council Formas for funding, in the frame of the
320 GlobalHydroPressure project financed under the 2017 Joint Call of Water JPI (IC4WATER).

321 References

- 322 Andersson, J. C., Ali, A., Arheimer, B., Gustafsson, D., and Minoungou, B.: Providing peak river flow statistics and forecasting in the Niger
323 River basin, *Phys. Chem. Earth A/B/C*, 100, 3–12, <https://doi.org/10.1016/j.pce.2017.02.010>, 2017.
- 324 Arheimer, B., Pimentel, R., Isberg, K., Crochemore, L., Andersson, J. C. M., Hasan, A., and Pineda, L.: Global catchment mod-
325 elling using World-Wide HYPE (WWH), open data, and stepwise parameter estimation, *Hydrol. Earth Syst. Sci.*, 24, 535–559,
326 <https://doi.org/10.5194/hess-24-535-2020>, 2020.
- 327 Ashouri, H., Hsu, K.-L., Sorooshian, S., Braithwaite, D. K., Knapp, K. R., Cecil, L. D., Nelson, B. R., and Prat, O. P.: PERSIANN-CDR:
328 Daily Precipitation Climate Data Record from Multisatellite Observations for Hydrological and Climate Studies, *Bull. Amer. Meteor.*
329 *Soc.*, 96, 69–83, <https://doi.org/10.1175/bams-d-13-00068.1>, 2015.
- 330 Beck, H. E., van Dijk, A. I. J. M., Levizzani, V., Schellekens, J., Miralles, D. G., Martens, B., and de Roo, A.: MSWEP: 3-hourly
331 0.25° global gridded precipitation (1979–2015) by merging gauge, satellite, and reanalysis data, *Hydrol. Earth Syst. Sci.*, 21, 589–615,
332 <https://doi.org/10.5194/hess-21-589-2017>, 2017.
- 333 Berg, P., Donnelly, C., and Gustafsson, D.: Near-real-time adjusted reanalysis forcing data for hydrology, *Hydrol. Earth Syst. Sci.*, 22,
334 989–1000, <https://doi.org/10.5194/hess-22-989-2018>, 2018.
- 335 Chen, M., Shi, W., Xie, P., Silva, V. B. S., Kousky, V. E., Wayne Higgins, R., and Janowiak, J. E.: Assessing objective techniques for
336 gauge-based analyses of global daily precipitation, *J. Geophys. Res. Atm.*, 113, D04 110, <https://doi.org/10.1029/2007JD009132>, 2008.
337 CPCtemp: <https://www.esrl.noaa.gov/psd/data/gridded/data.cpc.globaltemp.html>, 2017.
- 338 Cucchi, M., Weedon, G. P., Amici, A., Bellouin, N., Lange, S., Schmied, H. M., Hersbach, H., and Buontempo, C.: WFDE5: bias adjusted
339 ERA5 reanalysis data for impact studies, *Earth Syst. Sci. Data Discuss.*, 12, 2097–2120, <https://doi.org/10.5194/essd-12-2097-2020>, 2020.
- 340 Fallah, A., Rakhshandehroo, G. R., Berg, P., O, S., and Orth, R.: Evaluation of precipitation datasets against local observations in southwestern
341 Iran, *Int. J. Climatol.*, <https://doi.org/10.1002/joc.6445>, 2020.
- 342 Fan, Y. and Van den Dool, H.: A global monthly land surface air temperature analysis for 1948–present, *J. Geophys. Res. Atm.*, 113, D1,
343 <https://doi.org/10.1029/2007JD008470>, 2008.
- 344 Funk, C., Peterson, P., Landsfeld, M., Pedreros, D., Verdin, J., Shukla, S., Husak, G., Rowland, J., Harrison, L., Hoell, A., and Michaelsen,
345 J.: The climate hazards infrared precipitation with stations—a new environmental record for monitoring extremes, *Sci. Data*, 2,
346 <https://doi.org/10.1038/sdata.2015.66>, 2015a.
- 347 Funk, C., Verdin, A., Michaelsen, J., Peterson, P., Pedreros, D., and Husak, G.: A global satellite-assisted precipitation climatology, *Earth*
348 *Syst. Sci. Data*, 7, 275–287, <https://doi.org/10.5194/essd-7-275-2015>, 2015b.
- 349 Giorgi, F. and Bi, X.: Updated regional precipitation and temperature changes for the 21st century from ensembles of recent AOGCM
350 simulations, *Geophys. Res. Lett.*, 32, <https://doi.org/10.1029/2005gl024288>, 2005.
- 351 Harris, I. C. and Jones, P. D.: CRU TS4.03: Climatic Research Unit (CRU) Time-Series (TS) version 4.03 of high-resolution gridded data of
352 month-by-month variation in climate (Jan. 1901– Dec. 2018), <https://doi.org/10.5285/10D3E3640F004C578403419AAC167D82>, 2019.
- 353 Hersbach, H., Bell, B., Berrisford, P., Hirahara, S., Horányi, A., Muñoz-Sabater, J., Nicolas, J., Peubey, C., Radu, R., Schepers, D., Simmons,
354 A., Soci, C., Abdalla, S., Abellan, X., Balsamo, G., Bechtold, P., Biavati, G., Bidlot, J., Bonavita, M., Chiara, G., Dahlgren, P., Dee,
355 D., Diamantakis, M., Dragani, R., Flemming, J., Forbes, R., Fuentes, M., Geer, A., Haimberger, L., Healy, S., Hogan, R. J., Hólm, E.,
356 Janisková, M., Keeley, S., Laloyaux, P., Lopez, P., Lupu, C., Radnoti, G., Rosnay, P., Rozum, I., Vamborg, F., Villaume, S., and Thépaut,
357 J.-N.: The ERA5 global reanalysis, *Quart. J. Roy. Meteor. Soc.*, 146, 1999–2049, <https://doi.org/10.1002/qj.3803>, 2020.

358 Huebener, H. and Körper, J.: Changes in Regional Potential Vegetation in Response to an Ambitious Mitigation Scenario, *J Environ Prot*, 04,
359 16–26, <https://doi.org/10.4236/jep.2013.48a2003>, 2013.

360 Hundecha, Y., Arheimer, B., Donnelly, C., and Pechlivanidis, I.: A regional parameter estimation scheme for a pan-European multi-basin
361 model, *J. Hydrol. Regional Studies*, 6, 90–111, <https://doi.org/10.1016/j.ejrh.2016.04.002>, 2016.

362 Joyce, R. J., Janowiak, J. E., Arkin, P. A., and Xie, P.: CMORPH: A Method that Produces Global Precipitation Estimates from Passive
363 Microwave and Infrared Data at High Spatial and Temporal Resolution, *J. Hydrometeorol.*, 5, 487–503, <https://doi.org/10.1175/1525->
364 7541(2004)005<0487:camtpg>2.0.co;2, 2004.

365 Lindström, G., Pers, C., Rosberg, R., Strömqvist, J., and Arheimer, B.: Development and test of the HYPE (Hydrological Pre-
366 dictions for the Environment) model - A water quality model for different spatial scales, *Hydrol. Res.*, 41.3-4, 295–319,
367 <https://doi.org/10.2166/nh.2010.007>, 2010.

368 Schneider, U., Becker, A., Finger, P., Meyer-Christoffer, A., and Ziese, M.: GPCC Full Data Monthly Version 2018.0 at 0.25: Monthly Land-
369 Surface Precipitation from Rain-Gauges built on GTS-based and Historic Data, https://doi.org/10.5676/DWD_GPCC/FD_M_V2018_025,
370 2018a.

371 Schneider, U., Becker, A., Finger, P., Meyer-Christoffer, A., and Ziese, M.: GPCC Monitoring Product Version 6.0 at
372 1.0: Near Real-Time Monthly Land-Surface Precipitation from Rain-Gauges based on SYNOP and CLIMAT Data,
373 https://doi.org/10.5676/DWD_GPCC/MP_M_V6_100, 2018b.

374 Stillman, S. and Zeng, X.: Development of a 0.5° global monthly raining day product from 1901 to 2010, *Geophys. Res. Lett.*, 43, 9704–9711,
375 <https://doi.org/10.1002/2016gl070244>, 2016.

376 Weedon, G., Gomes, S., Viterbo, P., Shuttleworth, W., Blyth, E., Österle, H., Adam, C., Bellouin, N., Boucher, O., and Best, M.: Creation
377 of the watch forcing data and its use to assess global and regional reference crop evaporation over land during the twentieth century, *J.*
378 *Hydrometeorol.*, 12, 823–848, <https://doi.org/10.1175/2011JHM1369.1>, 2011.

379 Weedon, G. P., Balsamo, G., Bellouin, N., Gomes, S., Best, M. J., and Viterbo, P.: The WFDEI meteorological forcing data set: WATCH
380 Forcing Data methodology applied to ERA-Interim reanalysis data, *Water Resour. Res.*, 50, 7505–7514, 2014.